Journal of Catalysis 260 (2008) 329–341

Contents lists available at ScienceDirect

Journal of Catalysis

www.elsevier.com/locate/jcat

The synthesis of highly dispersed noble and base metals on silica via strong electrostatic adsorption: I. Amorphous silica

Ling Jiao, John R. Regalbuto *

Department of Chemical Engineering, University of Illinois at Chicago, 810 S Clinton St, Chicago, IL 60607, USA

ARTICLE INFO

Article history:
Received 7 March 2008
Revised 30 August 2008
Accepted 19 September 2008
Available online 31 October 2008

Keywords:
Catalyst preparation
Synthesis
Strong electrostatic adsorption
Platinum
Palladium
Ruthenium
Copper
Cobalt
Nickel
Ammine
Silica
Point of zero charge
PZC

ABSTRACT

To determine the correlation between strong electrostatic interaction during impregnation and the high dispersion of reduced metals, a series of silica-supported noble and base metal catalysts prepared by strong electrostatic adsorption (SEA) was compared with the traditional incipient wetness impregnation (IWI) method. Metal ammine complexes ($[Pd(NH_3)_4]^{+2}$, $[Cu(NH_3)_4]^{+2}$, $[Co(NH_3)_6]^{+3}$, $[Ru(NH_3)_6]^{+2}$, $[Ru(NH_3)_6]^{+3}$ and $[Ni(NH_3)_6]^{+2}$) were adsorbed onto amorphous silica at various pHs, and the corresponding metal uptakes were determined as a function of pH at fixed metal concentrations. The pH shifts relative to metal free control experiments were carefully monitored. The revised physical adsorption (RPA) model was used to simulate the adsorption process. The adsorption mechanism of metal ammine complexes over silica is reasonably well described as electrostatic interaction (physical adsorption) instead of ion exchange or chemical reaction. After impregnation, the appropriate reduction temperatures of the samples prepared via SEA and IWI methods were determined by temperature-programmed reduction (TPR), the particle size and distribution were measured from scanning transmission electron microscopy (STEM) images, and the metal distribution was analyzed by energy-dispersive X-ray spectroscopy (EDXS). X-ray photoelectron spectroscopy (XPS) also was used as a complementary technique to give information on the dispersion change before and after reduction. The results showed that the SEA method can be applied for many ammine complexes to synthesize well-dispersed metals over amorphous silica.

1. Introduction

Of all of the methods available to prepare metal-supported catalysts, impregnation is the simplest, least expensive, and most prevalent. Impregnation can be termed wet or dry, depending on whether the volume of impregnating solution is greater than or equal to the pore volume of the support. Dry impregnation often is termed incipient wetness impregnation (IWI). With wet impregnation (WI) when pH is not controlled, the pH of the impregnating solution can vary quite dramatically and often ends up near the support point of zero charge (PZC), at which point no metal precursor–support interaction occurs [1]. After impregnation, various drying and pretreatment steps can be used to remove the metal ligands and to reduce the metal to its catalytically active state.

Recent progress has been made in catalyst impregnation through fundamental studies of the adsorption process. A landmark work is the postulation of Brunelle that the adsorption of noble metal complexes onto common oxides supports was essentially coulombic in nature [2]. The hydroxyl groups that populate oxide surfaces become protonated and thus positively charged below a characteristic pH value or become deprotonated and thus negatively charged above the characteristic pH value. The pH at which the hydroxyl groups are neutral is termed the PZC. A simple intuitive picture of this surface chemistry is depicted in Fig. 1. Brunelle cited many instances in which oxides placed in solutions at pH values below their PZC would adsorb such anions as hexachloroplatinate $[PtCl_6]^{-2}$, whereas at pH values above their PZC would adsorb such cations as platinum tetraammine $[(NH_3)_4Pt]^{+2}$. In either case, the metal complex might be considered to deposit

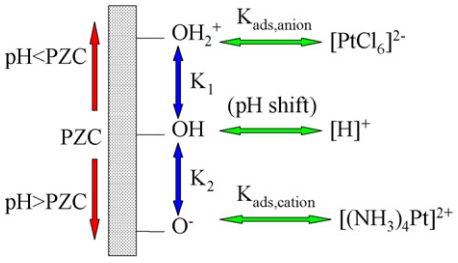

Fig. 1. Mechanism of electrostatic adsorption.

* Corresponding author.
E-mail address: jrr@uic.edu (J.R. Regalbuto).

0021-9517/$ – see front matter
doi:10.1016/j.jcat.2008.09.022

onto the surface via strong electrostatic adsorption (SEA). SEA is a special case of wet impregnation in which the final pH is targeted to the pH range in which the electrostatic interaction is strongest.

This mechanism has been ascertained for the uptake of cationic Pt ammine ($[Pt(NH_3)_4]^{+2}$) over a variety of amorphous silicas in previous work [3]. It also was demonstrated that catalysts prepared via SEA had a higher dispersion of Pt than those prepared via DI at the same metal loadings [4]. In the current study, it is desired to examine the applicability of the SEA method to other metal ammine complexes over a typical amorphous silica, which is the focus of this paper, and to mesoporous silicas, which were treated in the companion paper [5].

Silica-supported metal heterogeneous catalysts have been widely used in numerous studies of chemical and pharmaceutical production, environmental protection, pollution control, and energy production [6]. For example, Pd/SiO_2 catalyst can be used for hydrogenation of aldehydes to alcohols [7,8], Cu/SiO_2 catalyst is a good catalyst for methanol dehydrogenation [9,10], and Co/SiO_2 catalysts play an important role in the Fisher–Tropsch process [11].

The literature on the preparation of silica-supported Pd, Cu, Co, Ru, and Ni catalysts via impregnation [12–68] is quite voluminous and is summarized in Table S1 of the supporting material. For Pd, in most cases the catalysts were prepared via IWI, and the average particle size is usually large, except in those catalysts with very low metal loadings [20,21]. Particle size increases with increasing metal loading in IWI. The one study [16] that used ion exchange yielded particle sizes <2 nm at somewhat low loadings (<1.5 wt%).

For Cu catalysts, ion exchange was applied in more cases [24–26,28,30,31], and the metal particle sizes are generally smaller than those prepared at the same metal loading via IWI. In [30], for example, an IE preparation at 2.63 wt% gave a particle size of 16 Å, whereas IWI at 1.0 wt% yielded 100-Å particles. In the experiments of Toupance et al. [24,25], copper nitrate was used as the precursor, and the concentrated ammonium hydroxide was added to form copper tetraammine complexes and to adjust initial pH to 11.75. After impregnation for 24 h, the final pH shifted to a lower value, around 11.25. In [28,30], copper nitrate and ammonium hydroxide was used, and the pH was maintained constant at 11.9 and 11.5, respectively. In [31], the initial pH was 11, and the pH during impregnation was maintained at the desired value through periodic additions of ammonium nitrate. In all cases, the impregnation contact time usually exceeded 12 h. Cu catalysts prepared by IWI sometimes resulted in relatively small reduced metals [30].

For Co and Ru catalysts, it appears that only IWI or wet impregnation has been used, which generally results in large particles. Ion exchange has been used to synthesize a high metal loading (∼8%) Ni catalyst [64], and the average particle size of reduced metal is smaller than that prepared by IWI. In this literature, nickel amino complex synthesized from a solution of nickel nitrate in ammonia (30%) was used as a precursor, and the initial pH is given as 10.4. Although ion exchange has been used to create catalysts, and sometimes small metal particles result after reduction, few researchers have paid attention to the pH shift during impregnation, which can be dramatic and often is an important factor in the uptake of metal complexes over silica and the formation of strong interaction during impregnation.

The hypothesis behind the SEA approach to catalyst preparation is that monolayer adsorption of metal complexes via strong electrostatic adsorption can lead to small metal particles when the complexes are reduced. To extend the SEA method to the synthesis of other silica-supported noble and base metal catalysts, and further investigate the correlation between strong electrostatic interaction and highly dispersed metals on reduced catalysts, Pd/SiO_2, Cu/SiO_2, Co/SiO_2, Ru/SiO_2 and Ni/SiO_2 were prepared via strong electrostatic adsorption and compared with those prepared via the traditional dry impregnation method. The appropriate reduction temperature was determined by temperature-programmed reduction (TPR), the particle size and its distribution was determined by scanning transmission electron microscopy (STEM), and the metal distribution was demonstrated by energy-dispersive X-ray spectroscopy (EDXS). X-ray photoelectron spectroscopy (XPS) was used as a complementary technique to give information on the change in dispersion after reduction. The successful demonstration of the SEA method will yield a rational procedure for the cheap, simple, and scalable preparation of highly dispersed supported catalysts, even at relatively high metal loadings.

2. Experimental

The silica Vn-3S (surface area, 175 m^2/g; pore volume, 2.6 cm^3/g) was a commercial product from Degussa. The as-received PZC of the silica was 6.2, typical of precipitated silica with alkali impurities [3]. It was washed with 0.001 M nitric acid, shaken for 1 h, and then filtered, rinsed copiously with deionized water to remove any residual Na, dried overnight at 373 K, and calcined at 773 K for 3 h. The PZC of the washed silica was decreased to that of alkali-free silica, around 4.0 [3].

Palladium(II) tetraammine chloride monohydrate ($Pd(NH_3)_4Cl_2$, 99.9%), copper(II) tetraammine sulfate ($Cu(NH_3)_4SO_4$, 98%), cobalt (III) hexaammine chloride ($Co(NH_3)_6Cl_3$, 99%), ruthenium(II) hexaammine chloride ($Ru(NH_3)_6Cl_2$, 99.9+%), ruthenium(III) hexaammine chloride ($Ru(NH_3)_6Cl_3$, 98%), and nickel(II) hexaammine chloride ($Ni(NH_3)_6Cl_2$, 99.999%) precursors were obtained from Aldrich. These are designated PdTA, CuTA, CoHA, Ru(II)HA, Ru(III)HA, and NiHA, respectively. Stock solutions of the metal ammine complexes were prepared by placing the desired quantity of metal ammine complexes in a volumetric flask. For the Cu(II) and Ru(II) ammine complexes, concentrated ammonium hydroxide (NH_4OH, 14.8 M, from Fisher) was added to dissolve the precipitate formed. The solutions were then diluted to the correct volume. Copper tetraammine complex also was prepared by adding ammonium hydroxide into a copper nitrate ($Cu(NO_3)_2{\cdot}2.5H_2O$, 98%, from Aldrich) solution. Metal concentrations were measured by ICP (Perkin Elmer Optima 2000) before and after contact with silica to determine the metal uptake. The accuracy of ICP measurements was improved by using a multi-wavelength calibration, yttrium as an internal standard, multiple replicate data, and the radial analysis mode.

In metal-free pH shift control experiments, washed silica was weighed out to achieve two separate surface loadings (m^2 oxide per liter of solution) of 1000 and 10,000 m^2/L for 50 mL of solution. Acid and base solutions were created at various pH values in the range of 1–13 using HNO_3 and NaOH. Then 50 mL of each solution was added to the silica in 60-mL polypropylene bottles (from Fisher). The solutions were shaken for 1 h. Final pH measurements were taken using a general combination pH electrode. The initial and final pH measurements were then plotted with initial pH on the *x*-axis, and the final pH was plotted on the *y*-axis (pH shift plots).

Uptake–pH surveys were conducted in 60-mL polypropylene bottles containing 50 mL of 200 ppm metal solutions and various masses of silica such that surface loadings were 1000 m^2/L for all silicas. Metal solutions of initial pH of about 4–13 were used. Silica-free control experiments were conducted in parallel with each adsorption run. After the solutions were pipetted into bottles containing the silica, the suspensions were placed on an orbital shaker for 1 h, after which 5-mL portions were filtered (Biohit 22 μm) for ICP analysis. pH measurements also were made at this time. A 1-h adsorption time has been shown to allow plenty of time for adsorption equilibrium [3]; rapid Pt tetraammine adsorption kinetics (equilibrium uptake within 10 min) are demonstrated in the companion paper [5].

Table 1
Catalyst preparation methods and metal percentages.

Preparation method	Precursor	wt%	Reduction temp. (°C)
SEA	$Pd(NH_3)_4Cl_2$	2.2, 1.7, 1.1	200
SEA	$Cu(NH_3)_4SO_4$	2.8, 2.1, 1.4	400
SEA	$Co(NH_3)_6Cl_3$	1.8, 1.4, 0.9	800
SEA	$Ru(NH_3)_6Cl_2$	2.7, 2.0, 1.4	450
SEA	$Ru(NH_3)_6Cl_3$	3.0, 2.3, 1.5	450
SEA	$Ni(NH_3)_6Cl_2$	1.6, 1.2, 0.8	500
DI	$Pd(NH_3)_4Cl_2$	2.2, 1.7, 1.1	200
DI	$Cu(NO_3)_2$	2.8, 2.1, 1.4	400
DI	$Co(NH_3)_6Cl_3$	1.8, 1.4, 0.9	450
DI	$Ru(NH_3)_6Cl_3$	3.0, 2.3, 1.5	450
DI	$RuCl_3$	3.0, 2.3, 1.5	200
DI	$Ni(NO_3)_2$	1.6, 1.2, 0.8	500

The metal surface density, Γ_{metal}, is calculated at the concentration of metal adsorbed divided by the surface loading, that is,

$$\Gamma_{\text{metal}}\ (\mu\text{mol/m}^2) = \frac{(C_{\text{metal,initial}} - C_{\text{metal,final}})\ (\mu\text{mol/L})}{\text{SL}\ (\text{m}^2/\text{L})}.$$

In another set of adsorption experiments, uptake versus metal concentration was recorded at the optimal pH (about 11.5), using a surface loading of 1000 m^2/L.

2.1. Catalyst synthesis by SEA

The initial pHs of the various metal solutions were increased to around 12 by the addition of NaOH. (The corresponding final pH was 11.5.) For the $Ni(NH_3)_6Cl_2$ solution, only ammonia hydroxide can be applied to adjust pH; otherwise, precipitates occur. Then 0.5 g of silica was weighed out and added into the metal ammine complex solutions. After 1 h of shaking, the solid was filtered, washed, and then dried over night in flowing air. The metal elemental analysis determined by ICP.

2.2. Catalyst synthesis by DI

Various masses of metal complexes, determined to give metal loadings equivalent to the SEA preparations, were dissolved in 1.3 mL of deionized water and added to 0.5 g of silica. The catalysts were dried at 25 °C in a flowing air for 48 h. Samples were not calcined, but rather were reduced directly after drying. The metal percentages of these samples are listed in Table 1.

TPR was performed on the dried, unreduced samples in an AutoChem II 2920 automated catalyst characterization system. Approximately 0.1 g of each dried unreduced sample was loaded in a U-shaped Pyrex glass cell (10 cm long × 3.76 mm i.d.). Then 50 cm^3/min of argon gas was passed through the samples for 20 min to desorb moisture in the micropores of the silica. After this, the sample was reduced in 10% H_2/Ar (50 cm^3/min) to certain temperatures under temperature-programmed control. The heating rate was 10 °C/min. During the TPR, a liquid nitrogen/isopropanol trap was used to condense the product water in the effluent.

STEM measurements were made on both the dried unreduced samples and the reduced catalyst samples. Several milligrams of catalyst sample was added into isopropanol and sonicated for 10 min. A drop of the sample was then placed onto a carbon-coated copper grid (200 mesh, CuPK/100) from SPI Supplies. The grid-supported sample was then dried in an ultra-infrared lamp for at least 20 min until the isopropanol was evaporated thoroughly. The high-angle annular dark-field (HAADF) imaging, or Z-contrast imaging, was done using a JEOL electron microscope (JEM-2010F FasTEMm FEI) operated at 200 kV and an extracting voltage of 4500 V. STEM images of different dried unreduced and reduced samples were obtained. Typically, 12 different regions of a catalyst were imaged for particle size analysis.

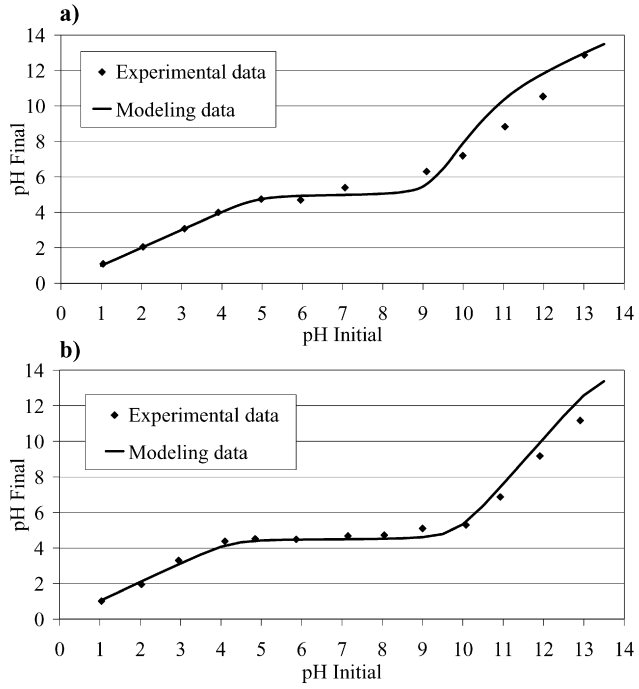

Fig. 2. Control experiments in metal-free solutions: (a) pH shift data for metal-free solutions contacted with silica at 1000 m^2/L (model fit obtained using PZC = 4.2, $\Delta pK = 7.0$), (b) at 10,000 m^2/L.

Approximately 500 particles of DI samples and 2000 particles of SEA samples were considered. The corresponding statistical data on particle size distribution was obtained using Particule2 software provided by Dr. Catherine Louis at the University Pierre et Marie Curie in Paris, and the average particle size of each reduced sample was calculated accordingly.

EDXS was performed on dried, unreduced catalyst samples in a JEOL JEM-2010F FasTEMm FEI electron microscope operated at 200 kV and an extracting voltage of 4500 V. The sample preparation was the same as that for the STEM analysis. Five different areas of a single grid-supported sample were chosen to be analyzed, and the corresponding metal loadings were recorded.

Both the dried unreduced and reduced catalyst samples were analyzed on a Kratos Axis 165 XRPS instrument. Beyond surface-sensitive elemental analysis, metal-to-silica ratios were used to estimate the metal dispersion of dried and reduced samples.

3. Results

Figs. 2a and 2b display the pH shift of silica at 1000 and 10,000 m^2/L without metal in solution. A wider plateau of final pH is seen at the higher surface loading, as expected [1]. The pH shift model, detailed in a previous paper [3], is represented as a solid line. In the application of the model to this system, the values of the parameters fitted to this date were PZC = 4.2, $\Delta pK = pK_2 - pK_1 = 7.0$, and $N_S = 5.0$ OH/nm^2, which agree with those values found previously for various amorphous silicas [3]. These parameters were used with no adjustment in later simulations of metal adsorption. The pH shift model reasonably describes the obtained pH shift data.

In adsorption surveys, the initial pH values were adjusted in the range of 4–13 for the adsorption of $[Pd(NH_3)_4]^{+2}$, $[Co(NH_3)_6]^{+3}$, $[Ru(NH_3)_6]^{+3}$, and $[Ru(NH_3)_6]^{+2}$ over silica. For the purchased and self-prepared $[Cu(NH_3)_4]^{+2}$ complexes, the adsorption surveys were performed at an initial pH of 10–13, because the copper ammine complex is not stable in the acidic pH range. For the $[Ni(NH_3)_6]^{+2}$ solution, a large quantity of concentrated ammonium

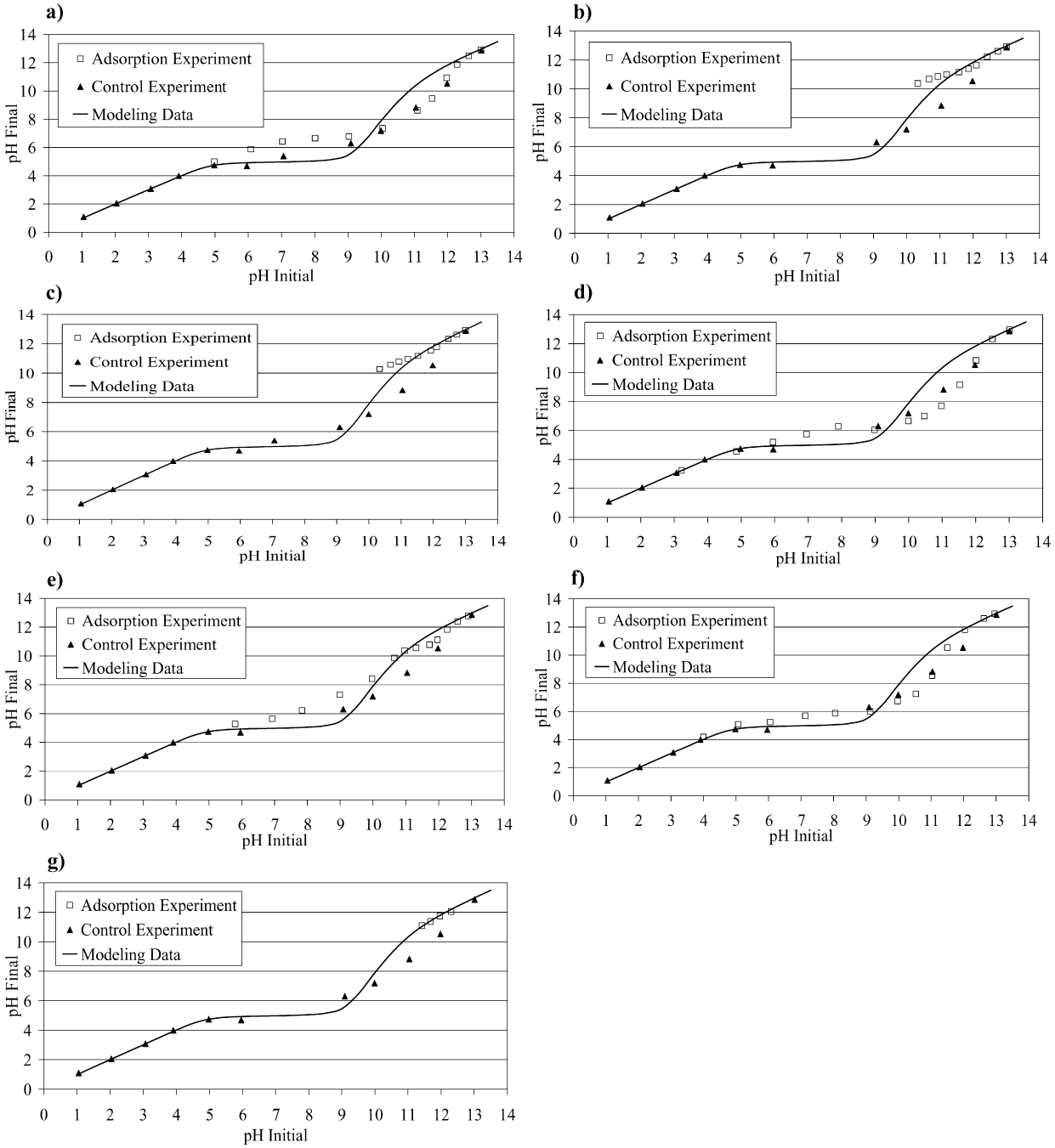

Fig. 3. pH shift after adsorption experiments: (a) $[Pd(NH_3)_4]^{+2}$ over silica, (b) purchased $[Cu(NH_3)_4]^{+2}$ over silica, (c) self-prepared $[Cu(NH_3)_4]^{+2}$ over silica, (d) $[Co(NH_3)_6]^{+3}$ over silica, (e) $[Ru(NH_3)_6]^{+2}$ over silica, (f) $[Ru(NH_3)_6]^{+3}$ over silica, (g) $[Ni(NH_3)_6]^{+2}$ over silica.

hydroxide was added to eliminate the precipitate formed and adjust the pH, because no sodium hydroxide could be applied. The ammonium hydroxide added made the solution strongly volatile, so the initial pH could be limited only in the range of 11–12.5.

Figs. 3a–3g display the pH shifts for various noble and base metal ammine adsorption experiments at 1000 m^2/L, with the pH shift model represented as the solid lines. The model used is identical to that used in the control experiment (without metal) displayed in Fig. 2a. The pH shift curves after adsorption display similar trends as those in the metal-free control experiment. In the initial pH range of 6–9, the final pHs of the adsorption of Pd, Co(III), Ru(II) and Ru(III) ammine complexes over silica are slightly higher than those in the metal-free control experiment. In the highly basic initial pH range of 10–12, the final pHs in the adsorption experiments of Pd, Co(III), and Ru(III) ammine complexes over silica fit the data of control experiment well. The final pHs of Ru(II) and Ni(II) ammine complexes adsorption are slightly higher than the data of the control experiment, whereas the final pHs of the purchased and self-prepared Cu ammine complexes adsorption are much higher than those in the metal-free control experiment.

Figs. 4a–4g display the adsorption curves over silica at 1000 m^2/L with the revised physical adsorption (RPA) model (discussed later) represented as the solid lines. The figures of the adsorption of $[Pd(NH_3)_4]^{+2}$, $[Co(NH_3)_6]^{+3}$, $[Ru(NH_3)_6]^{+3}$, and $[Ru(NH_3)_6]^{+2}$ over silica indicate that no adsorption occurs when the final pH is below the PZC of silica ($pH_{PZC} = \sim 4.0$). The silica adsorbs metal ammine complexes at pHs greater than pH_{PZC} and reaches a maximum uptake at a pH of around 11–11.5. Beyond a pH of 11.5,

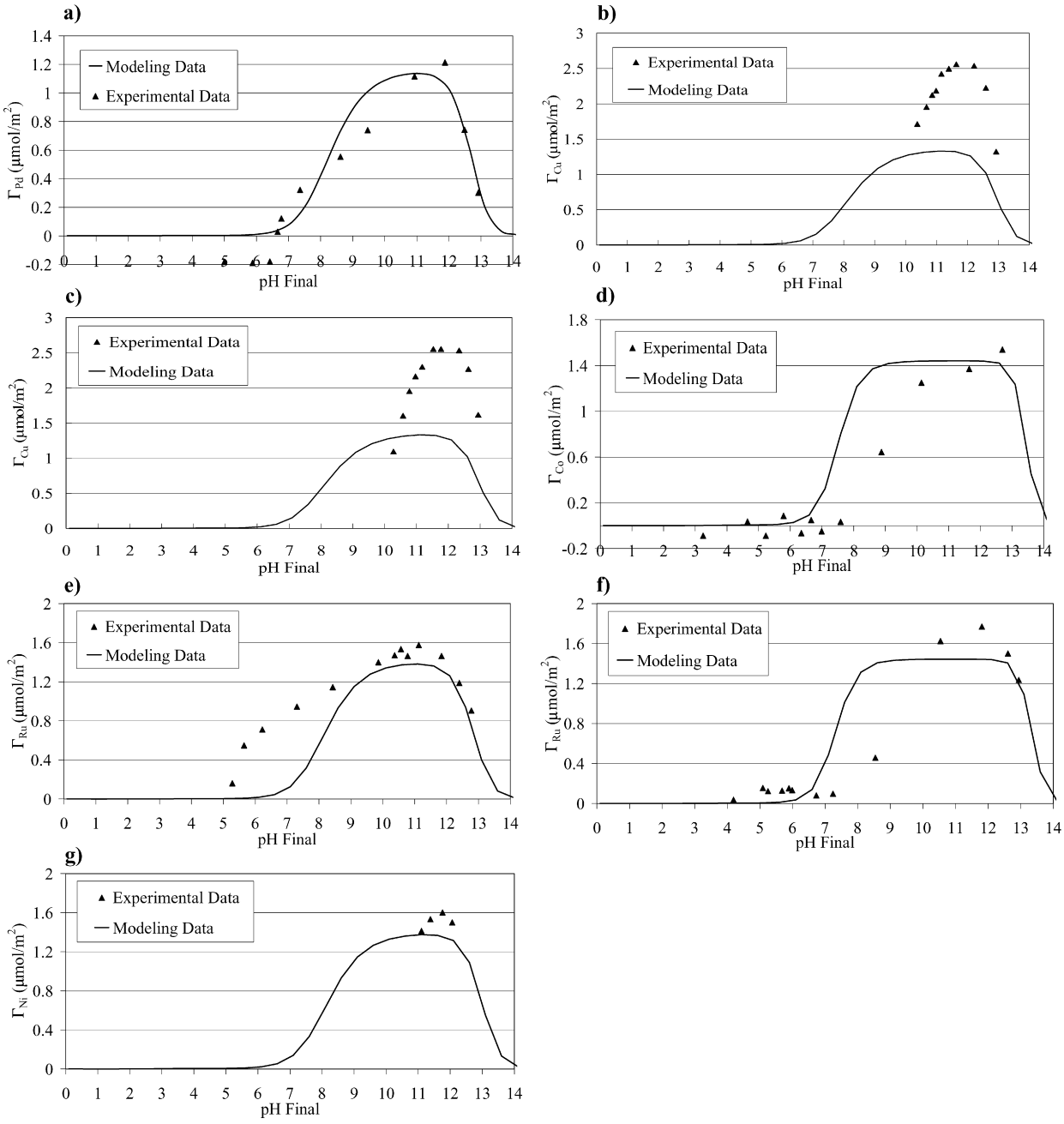

Fig. 4. Metal surface density vs. pH at surface loading 1000 m^2/L: (a) $[Pd(NH_3)_4]^{+2}$ over silica, (b) purchased $[Cu(NH_3)_4]^{+2}$ over silica, (c) self-prepared $[Cu(NH_3)_4]^{+2}$ over silica, (d) $[Co(NH_3)_6]^{+3}$ over silica, (e) $[Ru(NH_3)_6]^{+2}$ over silica, (f) $[Ru(NH_3)_6]^{+3}$ over silica, (g) $[Ni(NH_3)_6]^{+2}$ over silica (model fit obtained using PZC = 4.2, $\Delta pK = 7.0$, nhs = 1.5).

a decrease in adsorption is observed for all complexes except $[Co(NH_3)_6]^{+3}$, which continues to increase even in the extremely basic pH range.

Other adsorption experiments were performed while the final pH was kept constant (~11.5, maximum uptake) and the initial concentration of metal complexes was varied in solution. Figs. 5a–5e show the surface densities of metal adsorption (Γ_{metal}) versus initial metal concentrations (ppm) in solution for 1000 m^2/L, with the RPA model represented by a solid black line. The model is the same as that used previously. The metal concentration of 200 ppm corresponds to approximately one monolayer of metal in solution. The initial concentration is adjusted from 50 to around 800 ppm. The adsorption curves show that adsorption increases linearly at low initial metal concentrations, and then reaches a maximum adsorption at an initial concentration of around 200 ppm. After that, adsorption is retarded with the increase of initial concentration. For Pd, Co, and Ru(III) ammine complexes, the adsorption at high concentration of 600–800 ppm is even lower than that at lower concentration, which is caused by the effect of high ionic strength [3]. Once the silica is saturated, the additional PdTA remains in solution, increasing the ionic strength. For Cu, Ru(II) ammine complexes, there is excessive adsorption at high concentrations. This is believed to be caused by the formation of metal hydrates at the confluence of high metal concentration and low local pH (discussed later), and not by differences in the sizes of tetrahedrally coordinated versus octahedrally coordinated complexes.

The dried samples after impregnation were analyzed by XPS; the XPS spectra of N 1s are given in Fig. 6. In the XPS spectra of PdTA/SiO_2, CoHA/SiO_2, Ru(II)HA/SiO_2, and Ru(III)HA/SiO_2, N 1s peaks were observed at the binding energy of 398–399 eV. In

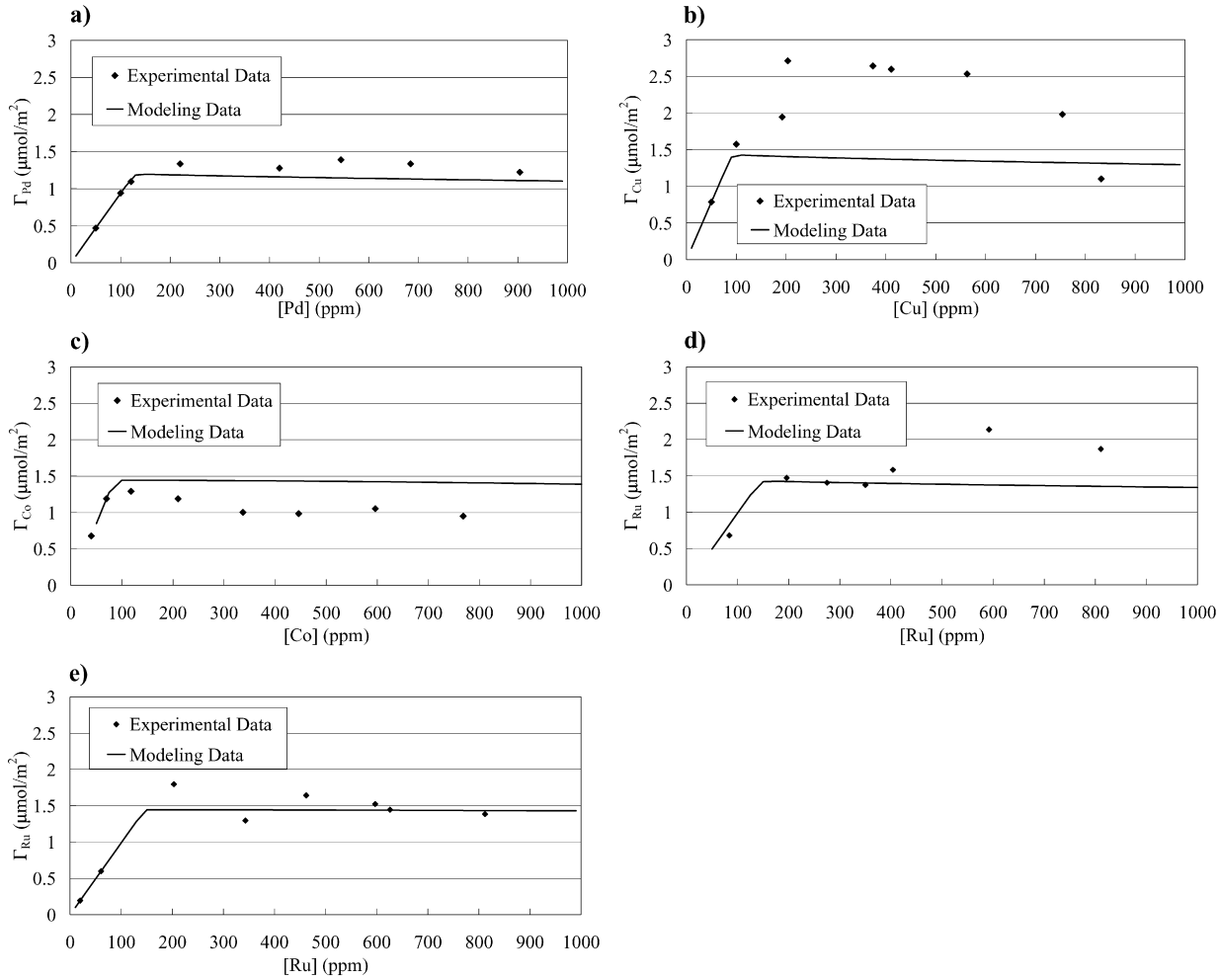

Fig. 5. Metal surface density at final pH 11.5 versus metal concentration at surface loading 1000 m^2/L: (a) $[Pd(NH_3)_4]^{+2}$ over silica, (b) purchased $[Cu(NH_3)_4]^{+2}$ over silica, (c) $[Co(NH_3)_6]^{+3}$ over silica, (d) $[Ru(NH_3)_6]^{+2}$ over silica, (e) $[Ru(NH_3)_6]^{+3}$ over silica (model fit obtained using PZC = 4.2, ΔpK = 7.0, nhs = 1.5).

the XPS spectra of CoHA/SiO_2 (Fig. 6c), another N 1s peak occurred at the binding energy of 406 eV, which might occur from partial degradation of the ammine ligands. In the XPS spectra of Ru(II)HA/SiO_2 (Fig. 6d), a peak with a binding energy of 402 eV appeared. This was likely due to the addition of ammonia hydroxide and residue of NH_4^+ remaining on sample surface. The XPS spectra of CuTA/SiO_2 and NiHA/SiO_2 showed almost no N 1s, however, indicating the extensive conversion of adsorbed species.

The XPS metal/support ratios are given in Table 2. This ratio provides a measure of metal dispersion, especially in comparisons of different preparations with the same bulk metal composition. In general, the metal/support ratios of the SEA preparations started out high and did not diminish drastically after reduction. On the other hand, some DI preparations showed high initial dispersion (Cu, Pd, and Ni), but in all three cases, the metal/support ratio diminished to a much lower value after reduction than that of the corresponding SEA preparation. The initial dispersion of the Co, Ru(III) ammine, and Ru(II) chloride DI preparations started out low and remained low after reduction.

The TPR patterns of dried, unreduced catalyst samples are summarized in Fig. 7. The PdTA/SiO_2 TPR profile (Fig. 7a) is characterized by a sharp negative peak, with an ill-defined H_2 consumption occurring as a small positive peak after the main peak. There is a general consensus that Pd can adsorb H_2 to form Pd hydrides at ambient temperature [69,70]. The decomposition of a Pd hydride phase has been linked to the negative peak (hydrogen release) in the TPR profile [69–72]. The CuTA/SiO_2 TPR profile (Fig. 7b) has only one typical H_2 consumption peak regardless of whether CuTA or $Cu(NO_3)_2$ was applied as the precursor, which demonstrates that Cu^{2+} was reduced to metallic Cu^0 directly and there is no transient stage. The TPR profile of Co(III)HA/SiO_2 (Fig. 7c) typically shows two peaks, one due to the reduction of Co^{3+} to Co^{2+} and another due to the reduction of Co^{2+} to metallic Co^0 [73,74]. Nevertheless, only one peak occurs in the TPR patterns, probably because the low Co metal loading results in the merger of those two peaks. For the TPR profiles of Ru(III)HA/SiO_2 and $RuCl_3$/SiO_2 profiles (Fig. 7d), two obvious peaks are seen, one demonstrating the reduction of Ru^{3+} to Ru^{2+} and the other corresponding to the reduction of Ru^{2+} to metallic Ru^0. It is interesting to note that two obvious peaks also occur in the TPR profile of Ru(II)HA/SiO_2. This seems contradictory, because theoretically, only one peak should occur from Ru^{2+} to Ru^0. There may be a speciation change during the adsorption process, and the adsorbed cations are not only $Ru(NH_3)_6^{2+}$; we discuss this in detail later. Thus, the different adsorbed salts require two different reduction temperatures and lead to two peaks. The NiHA/SiO_2 TPR profile (Fig. 7e) gives one H_2 consumption peak, which predicts the reduction of Ni^{2+} to metallic Ni^0, whereas the $Ni(NO_3)_2$/SiO_2 TPR profile has a sharp H_2 consumption peak with a secondary peak and a gradual return to baseline. The main peak has been assigned to the decomposition of nickel nitrate to NiO with a subsequent reduction to Ni metal [75].

From all of the TPR patterns, a common trend is that the TPR patterns of the samples prepared via DI always give sharp, narrow H_2 peaks, whereas SEA usually gives much wider H_2 consumption

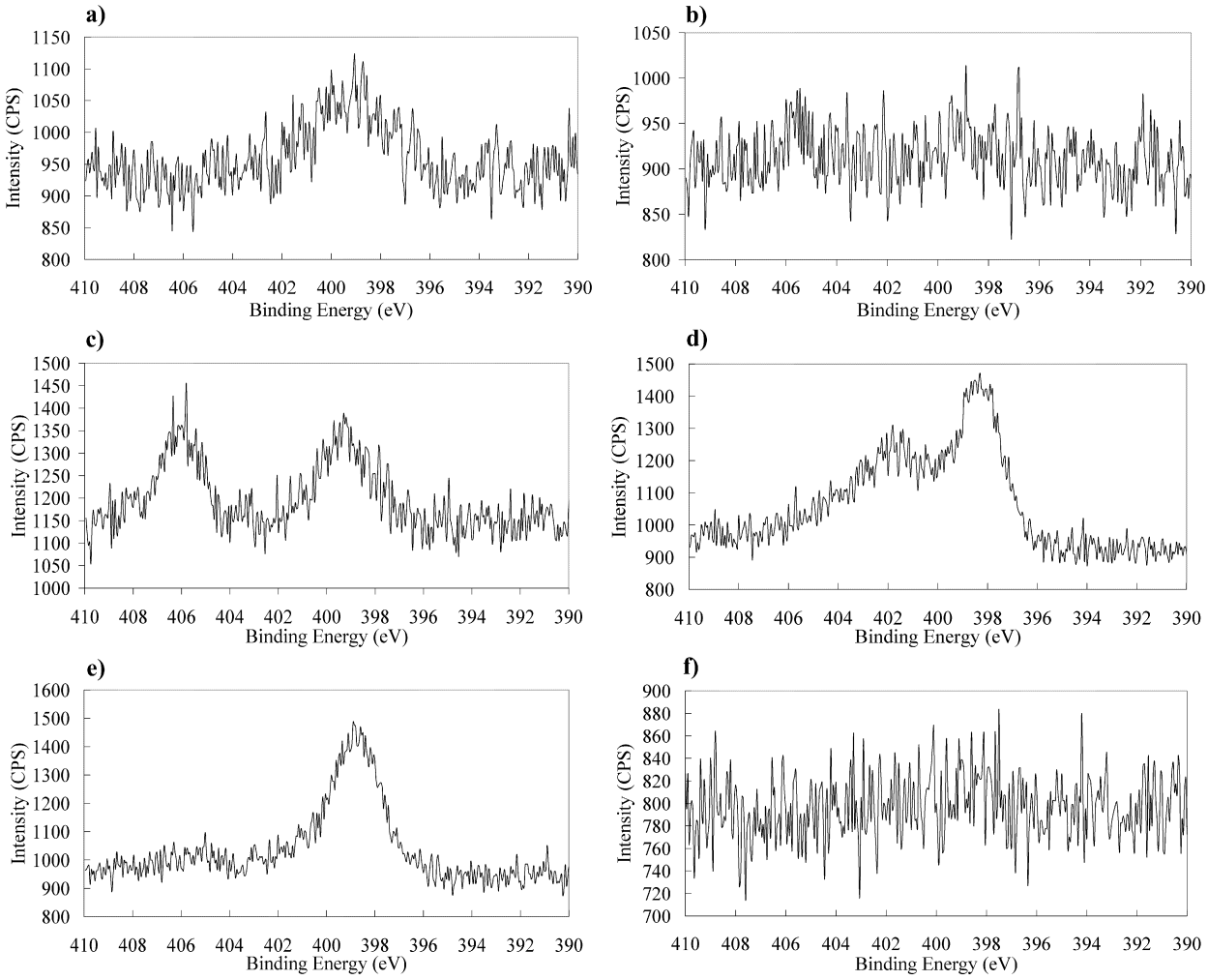

Fig. 6. N 1s XPS patterns of the samples prepared by SEA after impregnation: (a) PdTA/SiO_2; (b) CuTA/SiO_2; (c) CoHA/SiO_2; (d) Ru(II)HA/SiO_2; (e) Ru(III)HA/SiO_2; (f) NiHA/SiO_2.

Table 2
XPS data of unreduced and reduced samples prepared via SEA and DI methods.

Catalyst sample	Preparation method	wt%	Metal/Si (atomic ratio)	
			Unreduced	Reduced
Cu(II) ammine/SiO_2	SEA	2.8	0.051	0.040
$Cu(NO_3)_2/SiO_2$	DI	2.8	0.075	0.031
Co(III) ammine/SiO_2	SEA	1.8	0.027	0.020
Co(III) ammine/SiO_2	DI	1.8	0.010	0.010
Ru(II) ammine/SiO_2	SEA	2.7	0.033	0.024
Ru(III) ammine/SiO_2	SEA	3.0	0.027	0.021
Ru(III) ammine/SiO_2	DI	3.0	0.009	0.011
$RuCl_3/SiO_2$	DI	3.0	0.014	0.014
Pd(II) ammine/SiO_2	SEA	2.2	0.017	0.018
Pd(II) ammine/SiO_2	DI	2.2	0.016	0.007
Ni(II) ammine/SiO_2	SEA	1.6	0.038	0.031
$Ni(NO_3)_2/SiO_2$	DI	1.6	0.038	0.022

peaks. For the same precursor, the reduction temperature of SEA-prepared samples determined by TPR is significantly higher than that of DI-prepared samples. This is because the strong interaction between adsorbed species and silica exists in the SEA preparation process, which makes reduction of the metal precursor to the metallic state much more difficult and usually requires higher reduction temperatures and longer reduction times. We have noted the extraordinary stability of silica-adsorbed Co ammines in a previous paper [76].

The dried, unreduced catalyst samples were characterized with HAADF (Z-contrast) imaging. The results (not shown) indicate that metal ammine precursor complexes do not significantly agglomerate on the silica surface regardless of the impregnation method (SEA or DI) used. For $[Ru(NH_3)_6]^{+2}/SiO_2$, however, particles of about 5 nm do appear. These are attributed either to the instability of the complex to the STEM sample preparation method, which involves dissolution in ethanol, or to beam damage, because these particles are much larger than the particles of the reduced metal, as discussed below.

Fig. 8 shows representative HAADF images of reduced catalyst samples prepared via SEA at monolayer adsorption and the corresponding sample for DI preparations at the same metal loadings for Ru and Ni metals. A set of representative micrographs and particle size distributions for all metals (Pd, Cu, Co, Ru, and Ni) is given in the supplementary material, Fig. S2. Particles of the reduced catalyst samples are readily apparent for both the SEA and DI preparations. The average particle sizes for the SEA and DI preparations are summarized in Table 3. Metal particle sizes of the reduced catalysts prepared by SEA remain relatively small, and the size distributions are limited to a narrow range. Furthermore, the average particle sizes do not change much with an increase in metal loading. Reduced catalysts prepared by DI give much larger particle sizes. In a particular sample, the particle sizes occur in a wide distribution, and the average particle size increases significantly with increasing metal weight loading. The average particle size of the Co/SiO_2 catalyst synthesized via SEA is moderately large compared with the other SEA-prepared catalyst samples, be-

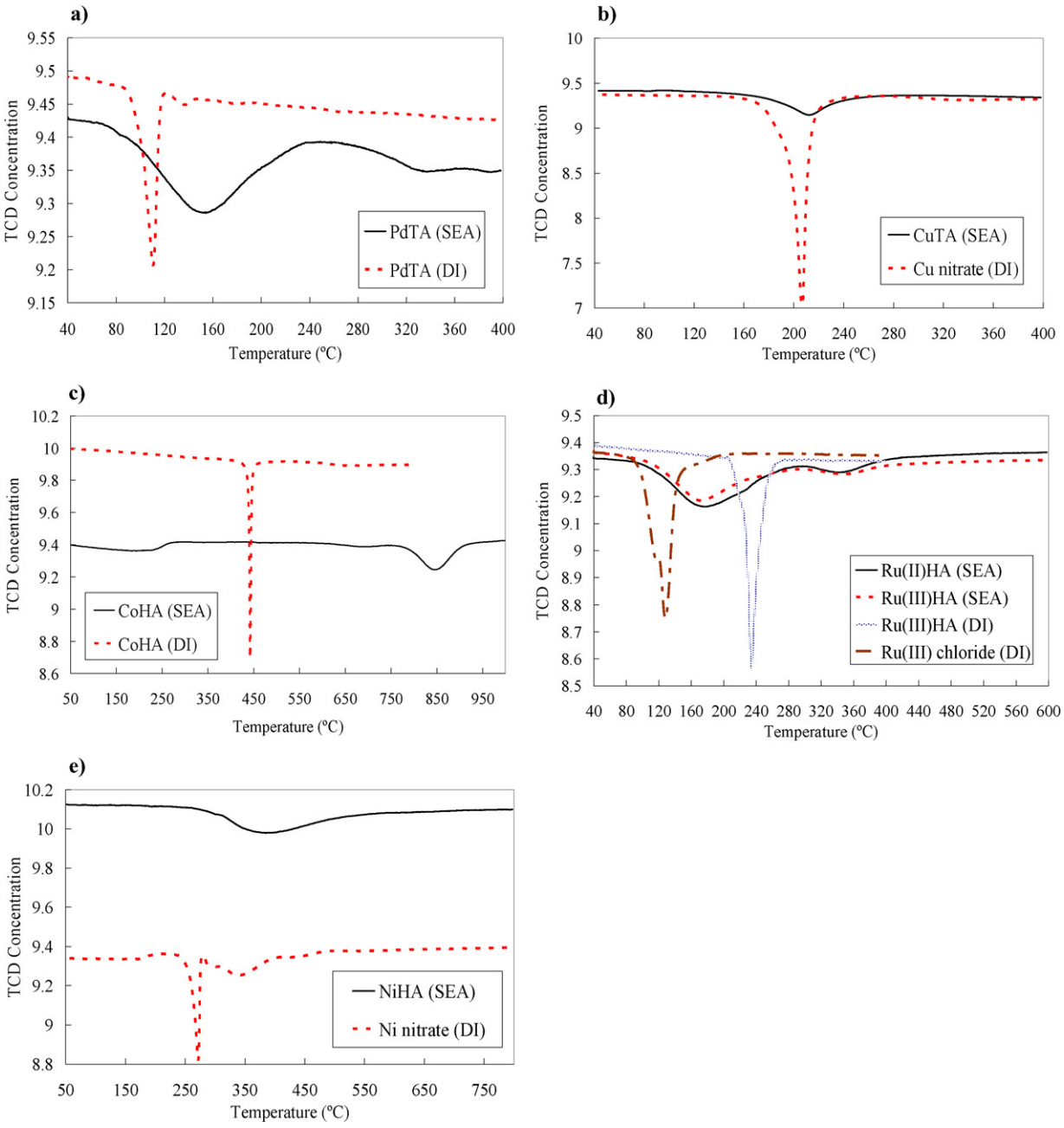

Fig. 7. TPR patterns of dried unreduced samples: (a) Pd/SiO_2, (b) Cu/SiO_2, (c) Co/SiO_2, (d) Ru/SiO_2, (e) Ni/SiO_2.

cause this sample requires a high reduction temperature (800 °C), at which agglomeration cannot be prevented.

To further investigate the homogeneity of metals deposited after the impregnation step, the average weight percentage and the standard deviation on the dried samples was obtained from EDXS for both SEA and DI samples. These data are given in the supplementary material, Table S2. Five different areas of approximately 0.5 μm^2 of each unreduced sample were chosen during the analysis, and the metal weight percentage of each specific area on which concentrated by the beamline was collected. The two Cu samples were omitted, because EDXS cannot distinguish the supported Cu complexes from the Cu grid. These results demonstrate that metal complexes tend to be evenly dispersed on the samples after SEA impregnation, and that the metal loading of various parts on a single catalyst sample are close to one another. However, the metal loadings of the samples after DI seemingly vary widely on different parts of a single sample; that is, with the DI method, adsorbed metal complexes are not evenly dispersed. Taking the dried, unreduced $CoHA/SiO_2$ sample as an example, the weight percentages determined by EDXS on the samples prepared via SEA and DI are compared in Fig. S2.

4. Discussion

4.1. Mechanism of metal ammine adsorption onto silica

Many previous researchers have described the adsorption process of metal ammine complexes over silica as an ion-exchange reaction [16,24–26,28,30,31,36,63]. Taking the Pd tetraammine complex as an example, the ion-exchange mechanism can be described in the following expression:

$$2(\mathrm{Si{-}O^-}, \mathrm{H^+}) + \left[\mathrm{Pd(NH_3)_4}\right]^{+2}, (\mathrm{OH^-})_2 \leftrightarrow (\mathrm{Si{-}O^-})_2, \left[\mathrm{Pd(NH_3)_4}\right]^{+2} + 2(\mathrm{H^+}, \mathrm{OH^-}).$$

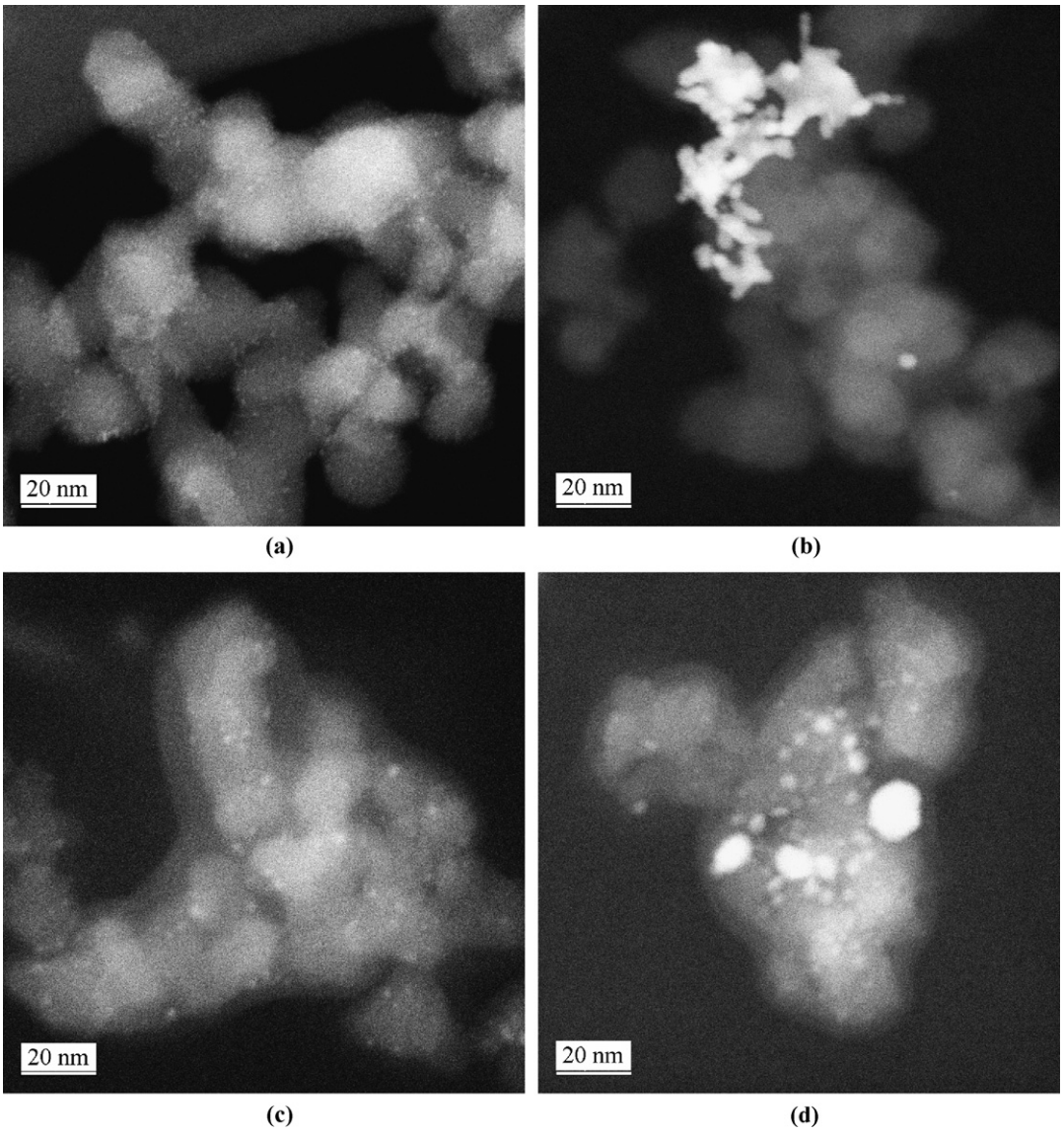

Fig. 8. Representative STEM images and corresponding particle distributions of reduced Ru and NI catalyst samples: (a) 3.0% Ru, SEA preparation; (b) 3.0% Ru, DI preparation; (c) 1.6% Ni, SEA preparation; (d) 1.6% Ni, DI preparation.

In the ion-exchange reaction, metal complexes can interact over a neutrally charged surface. If the adsorption mechanism of metal ammine complexes over silica is ion exchange, then the uptake should be expected to occur at the pH of the PZC of silica, because the surface is neutral, and the hydroxyl groups dominate silica surface species. But Fig. 4 shows that no metal ammine adsorption occurs in our experiments when the final pH equals the PZC of silica (around 4). At high pH ranges, the surface hydroxyl groups become deprotonated, and the number of OH groups decreases accordingly, inhibiting ion exchange. But the experimental results demonstrate that the maximum uptake occurs at a highly basic pH (11–12) when the surface is deprotonated, and this phenomenon contradicts the ion-exchange mechanism.

Furthermore, taking the Pd ammine complex as an example, ion exchange predicts that Pd ammines will deposit over the hydroxyl groups at the silica surface in a 1:2 stoichiometry. In our experiment, the maximum Pd uptake is about 1.2 μmol/m^2 at a final pH of 11.5 (initial pH 12). If the entire uptake were caused by ion exchange, then the protons released to the bulk solution should decrease the pH from an initial value of 12 to a final value of <3. The observed decrease to 11.5 is the same as that for a Pd-free control experiment and results from the proton exchange from the naturally acidic silanol groups with the solution. Both of these arguments run counter to an ion-exchange mechanism.

We believe that the adsorption mechanism is largely electrostatic, rather than ion exchange, based on the pH dependence of uptake. The adsorption survey of various noble and base ammine complexes over silica is displayed in Fig. 4. Again, taking the adsorption of Pd ammine complexes as an example, when the final pH of the solution is below the PZC of silica, the surface is protonated and positively charged, so it cannot attract $[Pd(NH_3)_4]^{+2}$, and thus no adsorption occurs. As the pH rises above the PZC of silica, the surface is deprotonated and negatively charged, and it begins to adsorb $[Pd(NH_3)_4]^{+2}$. The surface charge increases with the rise of pH, and the uptake increases accordingly. The maximum extent of adsorption for the cationic Pd ammine complex occurs when the final pH reaches 11.5. At higher pH, adsorption is retarded by the effect of high ionic strength, which effectively diminishes the value of the adsorption equilibrium constant [3]. The same uptake tendency can be observed in the adsorption experiments of almost all other metal ammine complexes over silica.

Table 3
Average particle size and standard deviation of the reduced catalysts prepared by SEA and DI.

Catalyst	Preparation method	Precursor	wt%	$T_{reduction}$ (°C)	Average diameter (Å)	σ (Å)
Pd/SiO_2	SEA	$Pd(NH_3)_4Cl_2$	1.1	200	15	3.4
			1.7	200	15	3.3
			2.2	200	16	3.9
	DI	$Pd(NH_3)_4Cl_2$	1.1	200	37	20
			1.7	200	44	25
			2.2	200	55	34
Cu/SiO_2	SEA	$Cu(NH_3)_4SO_4$	1.4	400	17	6.3
			2.1	400	23	6.0
			2.8	400	31	8.2
	DI	$Cu(NO_3)_2$	1.4	400	40	26
			2.1	400	89	74
			2.8	400	140	170
Co/SiO_2	SEA	$Co(NH_3)_6Cl_3$	0.9	800	37	15
			1.4	800	29	11
			1.8	800	43	17
	DI	$Co(NH_3)_6Cl_3$	0.9	450	27	9.1
			1.4	450	32	15
			1.8	450	74	70
Ru/SiO_2	SEA	$Ru(NH_3)_6Cl_2$	1.4	450	11	2.2
			2.0	450	11	2.5
			2.7	450	12	2.5
	SEA	$Ru(NH_3)_6Cl_3$	1.5	450	11	2.8
			2.3	450	11	2.0
			3.0	450	12	2.1
	DI	$Ru(NH_3)_6Cl_3$	1.5	300	34	15
			2.3	300	44	17
			3.0	300	130	47
	DI	$RuCl_3$	1.5	200	18	5.8
			2.3	200	22	7.4
			3.0	200	20	6.7
Ni/SiO_2	SEA	$Ni(NH_3)_6Cl_2$	0.8	500	17	3.8
			1.2	500	17	3.7
			1.6	500	17	3.6
	DI	$Ni(NO_3)_2$	0.8	500	24	9.3
			1.2	500	29	15
			1.6	500	32	17

The fits of the adsorption data in Fig. 4 to the RPA predictions are qualitatively correct and, in the case of Pd, Ru(III), and Ni, quantitatively reasonable. The RPA model works well in describing the uptake of Pt ammine on silica [3]. The RPA model parameters fit from the metal-free pH shift experiments of Fig. 2, and the size of the adsorbing complexes is estimated from literature data. Resonant anomalous X-ray reflectivity analysis on a model platinum tetraammine (PTA)/quartz crystal system was recently performed at the Advanced Photo Source at Argonne National Laboratory [77]. The results demonstrate that at the adsorbing PTA, complexes retain either one layer or two layers of water. Based on this finding, an average number of hydration sheaths (nhs) of 1.5 was used in the estimate of the radii of all of the metal ammine complexes. The radius of $[Pd(NH_3)_4]^{+2}$ is 2.55 Å, which comes from the literature [78]. This value is also applied to $[Ru(NH_3)_6]^{+3}$ and $[Ru(NH_3)_6]^{+2}$, because the atomic weights of Pd and Ru are similar. The radii of the other metal ammines are not available; thus, a rough estimation of 2.0 Å is applied for the radius of Cu, Co, and Ni ammines considering that the atomic weights of these metals are lower than that of Pd.

Deviations from a strictly electrostatic mechanism can be explained by instability or reactivity of the metal ammine complex. The discrepancy in Cu uptake has been addressed in a previous publication [79]; it was postulated that as they approach the adsorption plane, Cu ammine complexes respond to a local decrease in pH and form the bridged hydroxyl dimmers, as occurs in the bulk solution phase at lower pH. Metal adsorption density is inherently higher for the dimer than for the ammine complex.

The discrepancy between the Ru(II) data (Fig. 4e) and the RPA model may be explained by the instability of that complex. The XPS N 1s spectra (Fig. 6d) and microscopy studies of the dried precursors both indicate instability of the Ru(II) ammine complex. The TRP profiles for the Ru(II) complex is virtually identical to that of Ru(III), and the adsorption trends shown in Fig. 4e are actually better fit by the model for Ru(III) in Fig. 4f. It appears that the Ru(II) complexes are more like Ru(III) complexes in the solution conditions that we have used.

In the XPS data of Fig. 6, the $NiHA/SiO_2$ sample also exhibits no N. Although this conversion of Ni species does not significantly affect the adsorption density from that predicted, the adsorbing species may be hydroxylated or aquated. Unfortunately, with Ni, a wider range of pH, to allow better interpretation of pH trends, was not possible.

A comprehensive explanation for all of our results is that adsorption is predominantly electrostatic, and less stable adsorbates can respond to local changes in pH and concentration as adsorption proceeds.

4.2. Correlation of SEA with high dispersion of reduced metals

Metal precursors deposited by SEA appear to be evenly distributed across the surface, as determined from EDXS (Fig. S2 and Table S2). The metal species do not sinter significantly with reduction, as demonstrated by the relatively high XPS metal/support ratios shown in Table 2 and the small particle sizes revealed by STEM (Fig. 8 and Table 3). The DI-prepared samples show much higher variations in local concentrations (Table S2). Even when DI results in high precursor dispersion after impregnation, such as for Cu, Pd, and Ni in the XPS results of Table 2, the metals sinter significantly after reduction.

The dispersion of each metal was calculated from the average particle size based on STEM results (Table 3). Fig. 9 compares the metal dispersion catalysts synthesized by SEA and DI methods. From this comparison, we can see at the same metal loading, SEA always yields a much higher dispersion than DI. Metal particle size is only a mild function of metal weight loading for SEA-prepared materials (Table 3), but is a strong function of weight loading for DI-prepared metals.

At DI conditions, the surface of the support is negligibly charged, due to the tremendous buffering capacity of the support [1], whereas for SEA, the surface is strongly charged, and the precursors are deposited at the pH of the strongest electrostatic attraction. Dried precursors exist in an aqueous-like environment in which electrostatic attraction can exist [78]. It will take much more study to determine when electrostatic effects cease and what interactions take their place as heating and reduction occur, yet it is empirically clear that monolayers and submonolayers of metal ammine precursors deposited onto silica by SEA retain high dispersion after reduction. A necessarily high reduction temperature can adversely impact metal dispersion, as is seen in the case of cobalt. We have reported on the extreme stability of silica-supported Co ammines in a separate paper [76].

The average particle size of Pd on silica via SEA is about 16 Å at the metal loading of 2.2%, which is smaller than that in the literature survey [12–23]. The Cu catalyst (Cu% = 2.8%) prepared via SEA has an average particle size of around 30 Å, and other researchers also have obtained good results with the so-called “ion-exchange” method (which we believe is better described as electrostatic adsorption) [24,25]. The Co catalyst prepared via SEA requires a high reduction temperature, which leads to relatively large particle size of 40–50 Å. However, the literature shows that those catalysts prepared via IWI result in even larger particles [38–49], except for the

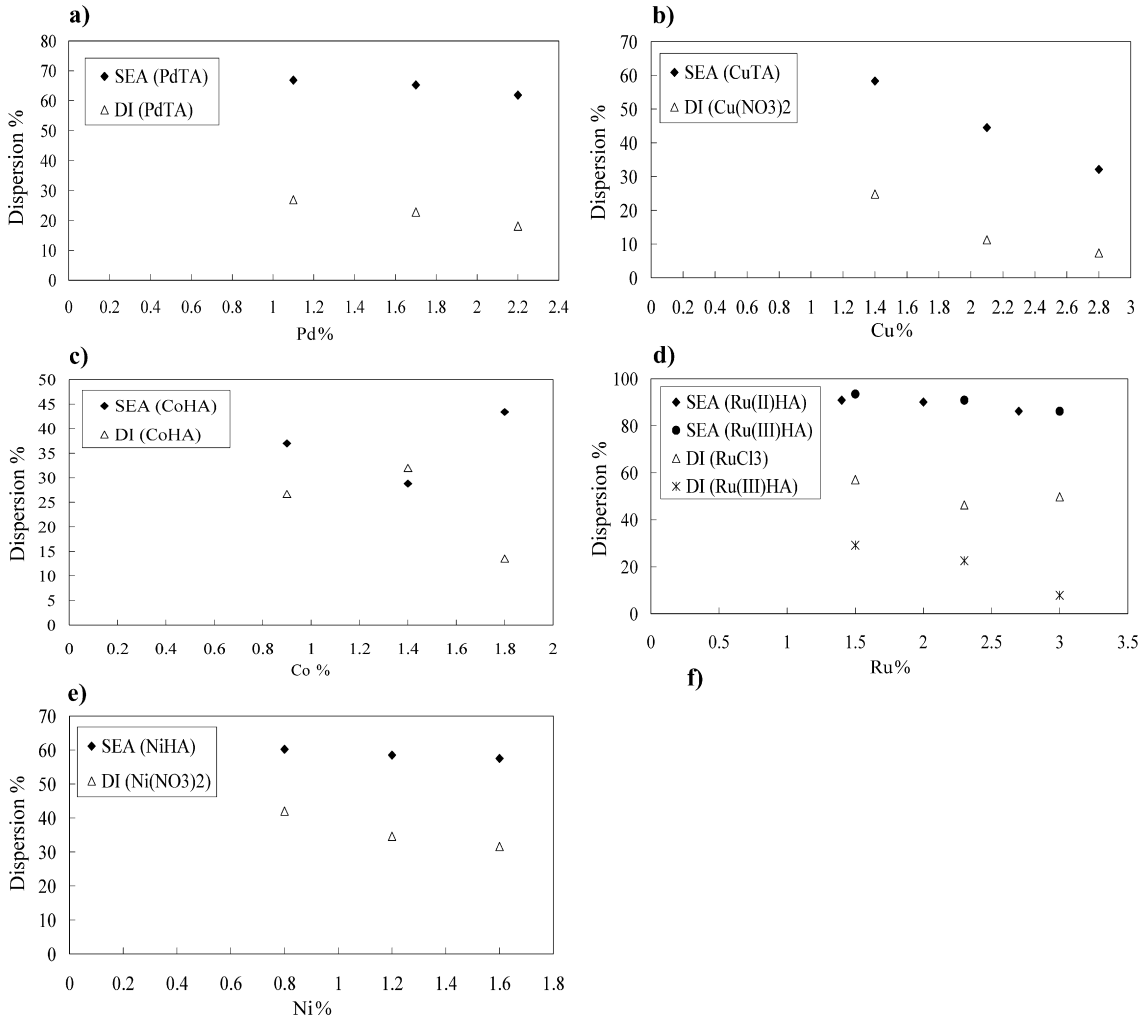

Fig. 9. Dispersion of silica-supported catalysts prepared via SEA and DI methods: (a) Pd/SiO_2, (b) Cu/SiO_2, (c) Co/SiO_2, (d) Ru/SiO_2, (e) Ni/SiO.

case in which $Co(CH_3COO)_2$ is applied as the precursor. Using SEA with Ru yields virtual nanoparticles at 11 or 12 Å. We believe these to be among the smallest Ru particles prepared to date [50–57]. Ni catalysts synthesized via SEA also show smaller sizes (<20 Å) than have been reported to date [58–67].

4.3. Practical considerations

SEA is a simple, scalable method that yields well-dispersed metals. Over silica, the pH range of optimal interaction can be seen in the volcano-shaped curves in Fig. 4 and appears to be in the range of 11–12 for all metals. This range is consistent with the pH values used for ion-exchange preparations [16,24–26,28,30,31, 36,63].

The optimal final pH can be easily obtained when working with powdered silica by using an initial pH that overcomes the buffering effect of the silica and leaves the pH high. For relatively thin slurries, such as the 1000 m^2/L used here, an initial pH of 12 suffices (as can be seen from the $pH_{initial}$–pH_{final} data in Figs. 2 and 3). For thicker slurries, the initial pH can be raised correspondingly. With powders, the final pH equilibrates within minutes, and the immediate drift toward lower pH minimizes the dissolution of silica. Silica dissolution has been reported for amorphous silicas [3] and for mesoporous silica [5] under similar impregnation conditions. The adsorption of the metal complexes into powdered silica also is complete within minutes [3,5], and a short contact time also minimizes Si dissolution. With formed catalysts, however, equilibration of pH and distribution of metal complexes require hours of contact [6]. In this case, to minimize Si dissolution, it likely will be advantageous to start by impregnation with a neutral solution, and then add base to increase the solution pH up to the desired value.

Perhaps the main limitation of the SEA method is that the metal weight loading that can be achieved in a single impregnation step is restricted to that amount of precursor that adsorbs in one monolayer. Using the monolayer limits shown in Figs. 4 and 5, the maximum metal loadings achievable by SEA are shown as a function of silica surface area in Fig. 10. For Pt, for example, a maximum uptake of about 0.9 μmol/m^2 [3] leads to about 6 wt% at 400 m^2/g, and 11 wt% at 750 m^2/g. Although Pd can be adsorbed at a higher density (1.2 μmol/m^2), its lower molecular weight results in lower mass loadings than for Pt. For cobalt, which adsorbs at 1.4 μmol/m^2, about 3 wt% can be adsorbed over a 400-m^2/g silica, whereas 6 wt% can be attained with 750 m^2/g of silica. SBA-15 materials, which commonly have surface areas approaching 1000 m^2/g, can be loaded at high metal dispersions with up to 14% Pt and 11% Pd in this fashion [3].

For higher metal loadings, somewhat lengthier and more complex catalyst preparation methods, such as deposition–precipitation [80–82] and controlled thermal decomposition [83], can be used to yield moderately small metal particles.

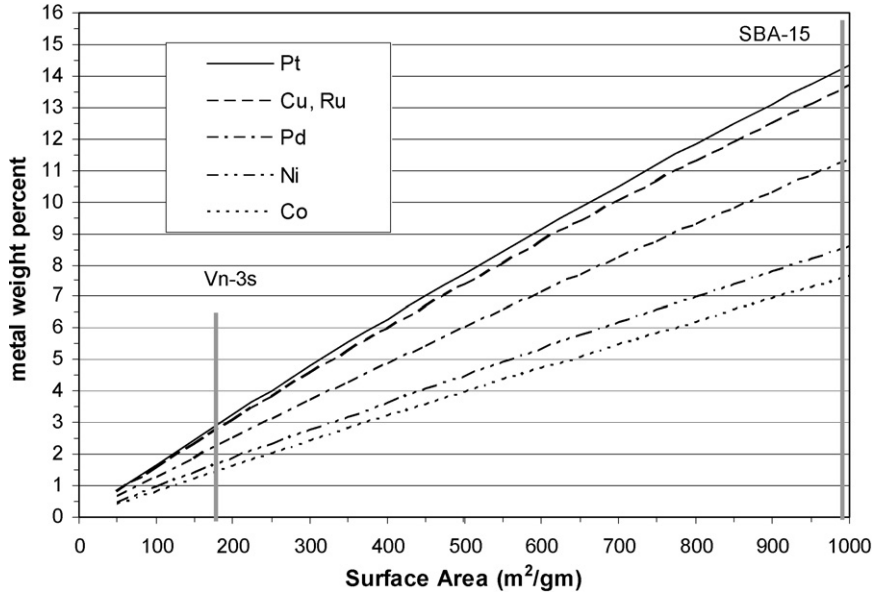

Fig. 10. Maximum calculated metal loadings via SEA versus silica surface area for the various metals.

5. Conclusion

The SEA method has been extended to the preparation of supported metal catalysts using the noble and base ammine complexes $[Pd(NH_3)_4]^{+2}$, $[Cu(NH_3)_4]^{+2}$, $[Co(NH_3)_6]^{+3}$, $[Ru(NH_3)_6]^{+2}$, $[Ru(NH_3)_6]^{+3}$, and $[Ni(NH_3)_6]^{+2}$. It appears that the high dispersion of electrostatically adsorbed ammine metal precursors is retained during reduction; a strong correlation between adsorption and high metal dispersion has been established. The SEA method appears to be a rational procedure for the cheap, simple, and scalable preparation of highly dispersed supported catalysts, even at relatively high metal loadings.

Acknowledgments

Support from the National Science Foundation (CTS-028181) is gratefully acknowledged.

Supplementary material

The online version of this article contains additional supplementary material.

Please visit DOI: 10.1016/j.jcat.2008.09.022.

References

[1] J. Park, J.R. Regalbuto, J. Colloid Interface Sci. 175 (1995) 239.
[2] J.P. Brunelle, Pure Appl. Chem. 50 (1978) 1211.
[3] M. Schreier, J.R. Regalbuto, J. Catal. 225 (2004) 190.
[4] J.T. Miller, A.J. Kropf, M. Schreier, J.R. Regalbuto, J. Catal. 225 (2004) 203.
[5] L. Jiao, J.R. Regalbuto, J. Catal. (2008), doi:10.1016/j.jcat.2008.09.023.
[6] J.R. Regalbuto, in: R. Richards (Ed.), Surface and Nanomolecular Catalysis, Taylor and Francis/CRC Press, Boca Raton, FL, 2006, p. 161.
[7] G. Del Angel, J.L. Benitez, J. Mol. Catal. 94 (1994) 409.
[8] D. Spielbauer, H. Zeilinger, H. Knozinger, Langmuir 9 (1993) 460.
[9] E.D. Guerreiro, O.F. Gorriz, J.B. Rivarola, L.A. Arrua, Appl. Catal. 165 (1997) 259.
[10] E.D. Guerreiro, O.F. Gorriz, G. Larsonborgmann, L.A. Arrua, Appl. Catal. A 204 (2000) 33.
[11] M. Voss, D. Borgmann, G. Wedler, J. Catal. 212 (2002) 10.
[12] J. Panpranot, K. Pattamakomsan, J.G. Goodwin Jr., P. Praserthdam, Catal. Commun. 5 (2004) 583.
[13] F. Pinna, F. Menegazzo, M. Signoretto, P. Canton, G. Fagherazzi, N. Pernicone, Appl. Catal. A 219 (2001) 195.
[14] J. Panpranot, O. Tangjitwattakorn, P. Praserthdam, J.G. Goodwin Jr., Appl. Catal. A 292 (2005) 322.
[15] S. Nait, M. Iwahashi, I. Kawakami, T. Miyao, Catal. Today 73 (2002) 355.
[16] B. Nohaira, C. Especela, G. Lafayea, P. Marecota, L.C. Hoang, J. Barbier, J. Mol. Catal. A 229 (2005) 117.
[17] S.H. Ali, J.G. Goodwin Jr., J. Catal. 176 (1998) 3.
[18] A.M. Kazi, B. Chen, J.G. Goodwin Jr., G. Marcelin, N. Rodriguez, R.T.K. Baker, J. Catal. 157 (1995) 1.
[19] N.S. Figoli, P.C. L'Argentiere, A. Arcoya, X.L. Seoane, J. Catal. 155 (1995) 95.
[20] G. Del Angel T, J.L. Benitez, J. Mol. Catal. 94 (1994) 409.
[21] M. Viniegra, G. Cordoba, R. Gomez, J. Mol. Catal. 58 (1990) 107.
[22] M.A. Aramendia, V. Borau, C. Jimenez, J.M. Marinas, A. Moreno, Colloids Surf. A 106 (1996) 161.
[23] M.A. Aramendia, V. Borau, I.M. Garcia, C. Jimenez, F. Lafont, A. Marinas, J.M. Marinas, F.J. Urbano, J. Catal. 187 (1999) 392.
[24] T. Toupance, M. Kermarec, C. Louis, J. Phys. Chem. B 104 (2000) 965.
[25] T. Toupance, M. Kermarec, J.-F. Lambert, C. Louis, J. Phys. Chem. B 106 (2002) 2277.
[26] R. Takahashi, S. Sato, T. Sodesawa, M. Kato, J. Sol–Gel Sci. Technol. 19 (2000) 715.
[27] P. Reyes, A. Figueroa, G. Pecchi, J.L.G. Fierro, Catal. Today 62 (2000) 209.
[28] E.D. Guerreiro, O.F. Gorriz, J.B. Rivarola, L.A. Arrfia, Appl. Catal. A 165 (1997) 259.
[29] H.Y. Chen, J. Lin, K.L. Tan, J. Li, Appl. Surf. Sci. 126 (1998) 323.
[30] E.D. Guerreiro, O.F. Gorriz, G. Larsen, L.A. Arrúa, Appl. Catal. A 204 (2000) 33.
[31] R.S. Rao, A.B. Walters, M.A. Vannice, J. Phys. Chem. B 109 (2005) 2086.
[32] A. Dandekar, M.A. Vannice, J. Catal. 178 (1998) 621.
[33] F.-W. Chang, W.-Y. Kuo, H.-C. Yang, Appl. Catal. A 288 (2005) 53.
[34] F.T. van de Scheur, L.H. Staala, Appl. Catal. A 108 (1994) 63.
[35] Y.-J. Tu, Y.-W. Chen, Ind. Eng. Chem. Res. 40 (2001) 5889.
[36] T. Toupance, M. Kermarec, C. Louis, J. Phys. Chem. B 104 (2000) 965.
[37] H.-W. Chen, J.-H. Lin, J. Phys. Chem. 199 (1996) 10353.
[38] M. Vo, D. Borgmann, G. Wedler, J. Catal. 212 (2002) 10.
[39] N. Tsubaki, Y. Zhang, S. Sun, H. Mori, Y. Yoneyama, X. Li, K. Fujimoto, Catal. Commun. 2 (2001) 311.
[40] E. Iglesia, S.L. Soled, R.A. Fiato, G.H. Via, J. Catal. 143 (1993) 345.
[41] T. Matsuzaki, K. Takeuchi, T.-A. Hanaoka, H. Arawaka, Y. Sugi, Appl. Catal. A 105 (1993) 159.
[42] K.E. Coulter, A.G. Sault, J. Catal. 154 (1995) 56.
[43] S.-W. Ho, Y.-S. Su, J. Catal. 168 (1997) 51.
[44] A. Thaib, G.A. Martin, P. Pinheiro, M.C. Schouler, P. Gadelle, Catal. Lett. 63 (1999) 135.
[45] A. Lapidus, A. Krylova, V. Kazanskii, V. Borovkov, A. Zaitsev, Appl. Catal. 73 (1991) 65.
[46] X. Qiu, N. Tsubaki, K. Fujimoto, J. Chem. Eng. Jpn. 34 (2001) 1366.
[47] G.-Z. Bian, N. Fujishita, T. Mochizuki, W.-S. Ning, M. Yamada, Appl. Catal. A 252 (2003) 251.
[48] L.M. Gandia, A. Diaz, M. Montes, J. Catal. 157 (1995) 461.
[49] S. Sun, N. Tsubaki, K. Fujimoto, Appl. Catal. A 202 (2000) 121.
[50] M. Lashdaf, A.O.I. Krause, M. Lindblad, M. Tiitta, T. Venäläinen, Appl. Catal. A 241 (2003) 65.
[51] V. Mazzieri, N. Figoli, F. Coloma-Pascual, P. L'Argentiere, Catal. Lett. 102 (2005) 79.
[52] B. Coq, P.S. Kumbhar, C. Moreau, P. Moreau, M.G. Warawdekar, J. Mol. Catal. 85 (1993) 215.

[53] P. Reyes, M.E. Konig, G. Pecchi, I. Concha, M. Lopez Granados, J.L.G. Fierro, Catal. Lett. 46 (1997) 71–75.
[54] S.Y. Chin, O.S. Alexeev, M.D. Amiridis, Appl. Catal. A 286 (2005) 157.
[55] G. Del Angel, C. Medina, R. Gomez, B. Rejai, R.D. Gonzalzez, Catal. Today 5 (1989) 395.
[56] H.-Y. Lin, Y.-W. Chen, Thermochim. Acta 419 (2004) 283.
[57] J.W. da-Silva, A.J.G. Cobo, Appl. Catal. A 252 (2003) 9.
[58] C. Crisafulli, S. Scirè, S. Minicò, L. Solarino, Appl. Catal. A 225 (2002) 1.
[59] X.-K. Li, W.-J. Ji, J. Zhao, S.-J. Wang, C.-T. Au, J. Catal. 236 (2005) 181.
[60] C. Hoang-Van, Y. Kachaya, S.J. Teichner, Y. Arnaud, J.A. Dalmon, Appl. Catal. 46 (1989) 281.
[61] H.M. Swaan, V.C.H. Kroll, G.A. Martin, C. Mirodatos, Catal. Today 21 (1994) 571.
[62] Y.H. Choi, W.Y. Lee, Catal. Lett. 67 (2000) 155.
[63] P. Wang, E. Tanabe, K. Ito, J. Jia, H. Morioka, T. Shishido, K. Takehira, Appl. Catal. A 231 (2002) 35.
[64] A. Gil, A. Diaz, L.M. Gandia, M. Montes, Appl. Catal. A 109 (1994) 167.
[65] M.A. Ermakova, D.Yu. Ermakov, G.G. Kuvshinov, L.M. Plyasova, J. Catal. 187 (1999) 77.
[66] A. Infantes-Molina, J. Mérida-Robles, P. Braos-García, E. Rodríguez-Castellón, E. Finocchio, G. Busca, P. Maireles-Torres, A. Jiménez-López, J. Catal. 225 (2004) 479.
[67] P.S. Kumbhar, Appl. Catal. A 96 (1993) 241.
[68] E. Iglesia, M. Boudart, J. Phys. Chem. 95 (1991) 7011.
[69] N. Nag, J. Phys. Chem. 105 (2001) 5945.
[70] M. Bonarowska, J. Pielaszek, V. Semikolenov, Z. Karpinski, J. Catal. 209 (2002) 528.
[71] G. Neri, M. Musolino, C. Milone, D. Pietropaolo, S. Galvagno, Appl. Catal. A 208 (2001) 307.
[72] M. Bonarowska, B. Burda, W. Juszczyk, J. Pielaszek, Z. Kowalczyk, Z. Karpinski, Appl. Catal. B 35 (2001) 13.
[73] C.L. Bianchi, Catal. Lett. 76 (2001) 155.
[74] I. Puskas, T.H. Fleisch, P.R. Full, J.A. Kaduk, C.L. Marshall, B.L. Meyers, Appl. Catal. A 311 (2006) 146.
[75] M.A. Keane, Appl. Catal. A 271 (2004) 109.
[76] L. D'Souza, L. Jiao, J.T. Miller, A.J. Kropf, J.R. Regalbuto, J. Catal. 248 (2007) 165.
[77] C. Park, P. Fenter, J.R. Regalbuto, Phys. Rev. Lett. 94 (2005) 76.
[78] N. Santhanam, T. Conforti, W. Spieker, J.R. Regalbuto, Catal. Today 21 (1994) 141.
[79] M. Schreier, S. Terens, L. Belcher, J.R. Regalbuto, Nanotech. 16 (2005) S582.
[80] A. Gil, A. Diaz, L.M. Gardia, M. Montes, Appl. Catal. A 109 (1994) 167.
[81] C. Louis, in: J.R. Regalbuto (Ed.), Catalyst Preparation: Science and Engineering, Taylor and Francis/CRC Press, Boca Raton, FL, 2007, p. 319.
[82] M.K. Van Der Lee, A. Van Jos Dillen, J.H. Bitter, K.P. de Jong, J. Am. Chem. Soc. 127 (2005) 13573.
[83] J.R.A. Sietsma, J.D. Meeldijk, J.P. Den Breejen, M. Versluijs-Helder, A.J. Van Dillen, P.E. de Jongh, K.P. de Jong, Angew. Chem. Int. Ed. 46 (2007) 4547.